Sensors & Actuators: B. Chemical 375 (2023) 132903

Contents lists available at ScienceDirect

Sensors and Actuators: B. Chemical

journal homepage: www.elsevier.com/locate/snb

PCA-TLNN-based SERS analysis platform for label-free detection and identification of cisplatin-treated gastric cancer

Dawei Cao [a], Hechuan Lin [a], Ziyang Liu [a], Jiaji Qiu [a], Shengjie Ge [b], Weiwei Hua [b], Xiaowei Cao [b,*], Yayun Qian [b,*], Huiying Xu [a,*], Xinzhong Zhu [a]

[a] College of Mathematics and Computer Science, Zhejiang Normal University, Jinhua 321004, China
[b] Institute of Translational Medicine, Medical College, Yangzhou University, Yangzhou 225001, China

ARTICLE INFO

Keywords:
Surface-enhanced Raman scattering
Gastric cancer
Au nano-hexagons
Principal component analysis
Two-layer nearest neighbour

ABSTRACT

Serum analysis is crucial for favourable prognosis of gastric cancer (GC) and for improving patient survival rates. However, it remains a challenge to develop an effective strategy to accurately identify differences in gastric cancer before and after treatment to guide efficacy evaluation. In this study, we combined surface-enhanced Raman scattering (SERS) with principal component analysis (PCA)-two-layer nearest neighbour (TLNN) to propose a promising serum analytical platform for label-free detection of cisplatin-treated GC mice. A microarray chip fabricated from Au nano-hexagon (AuNH) substrates was employed to measure the SERS spectra of the serum of GC mice at different treatment stages, and then a model for recognition of SERS spectra was constructed using a PCA-TLNN algorithm. The results revealed that the microarray chip exhibited superior portability, SERS activity, stability, and uniformity. Through PCA-TLNN, the GC mice at different treatment stages were successfully segregated, and several key spectral features for distinguishing different treatment stages were captured. The established PCA-TLNN model achieved satisfactory results, with an accuracy of over 97.5%, a sensitivity of over 90%, and a specificity of over 96.7%. Label-free serum SERS in combination with multivariate analysis could serve as a potential technique for the clinical diagnosis and staging of treatments.

1. Introduction

Gastric cancer (GC) is a common malignant tumour of the digestive system, and approximately 738,000 people die of GC each year worldwide, ranking second in cancer-related mortality [1–3]. The atypical early symptoms and high recurrence rate result in poor survival prognosis from GC, with five-year survival rates of approximately 20% over the past few decades [4,5]. Cisplatin, a first-generation platinum drug, has been widely used as a first-line therapy in clinical GC treatment. It can significantly accelerate apoptosis and bind to double-stranded DNA in cells, effectively preventing cell proliferation and division [6–8]. Moreover, cisplatin has a strong inhibitory effect on solid tumours. In the process of tissue carcinogenesis and during interaction between cisplatin and cancer cells, biomolecules, such as proteins, lipids, carbohydrates, and nucleic acids, in cells or tissues may change in structure, conformation, and content. Blood serum, as a type of body fluid, can provide rich information on human health; thus, analysis of body fluids can identify subtle changes in the post-biochemical composition during cisplatin therapy, guiding the application of cisplatin in antitumour therapy [9,10]. However, non-invasive efficacy assessment using conventional clinical techniques remains a challenge because it cannot provide sufficient information on changes occurring at the molecular level. Thus, there is an urgent requirement for fast, sensitive, and efficient methods to accurately identify differences before and after treatment of GC to guide efficacy assessment.

Raman scattering is a non-destructive and non-invasive optical analysis method based on the inelastic scattering of light, which can capture the molecular "fingerprint" information of biochemical substances; thus, the structure, content, and other information of biomolecules can be obtained by analysing unique Raman spectral peak position and peak intensity information [11–15]. However, it is difficult to obtain a high signal-to-noise Raman signal for biomolecules in practical detection because of the small inherent Raman scattering cross-section of a single molecule. Surface-enhanced Raman scattering (SERS) is a novel optical sensing technology developed based on Raman scattering that can significantly amplify signal intensity compared to

* Corresponding authors.
E-mail addresses: cxw19861121@163.com (X. Cao), yyqian@yzu.edu.cn (Y. Qian), xhy@zjnu.edu.cn (H. Xu).

https://doi.org/10.1016/j.snb.2022.132903
Received 23 August 2022; Received in revised form 15 October 2022; Accepted 24 October 2022
Available online 27 October 2022

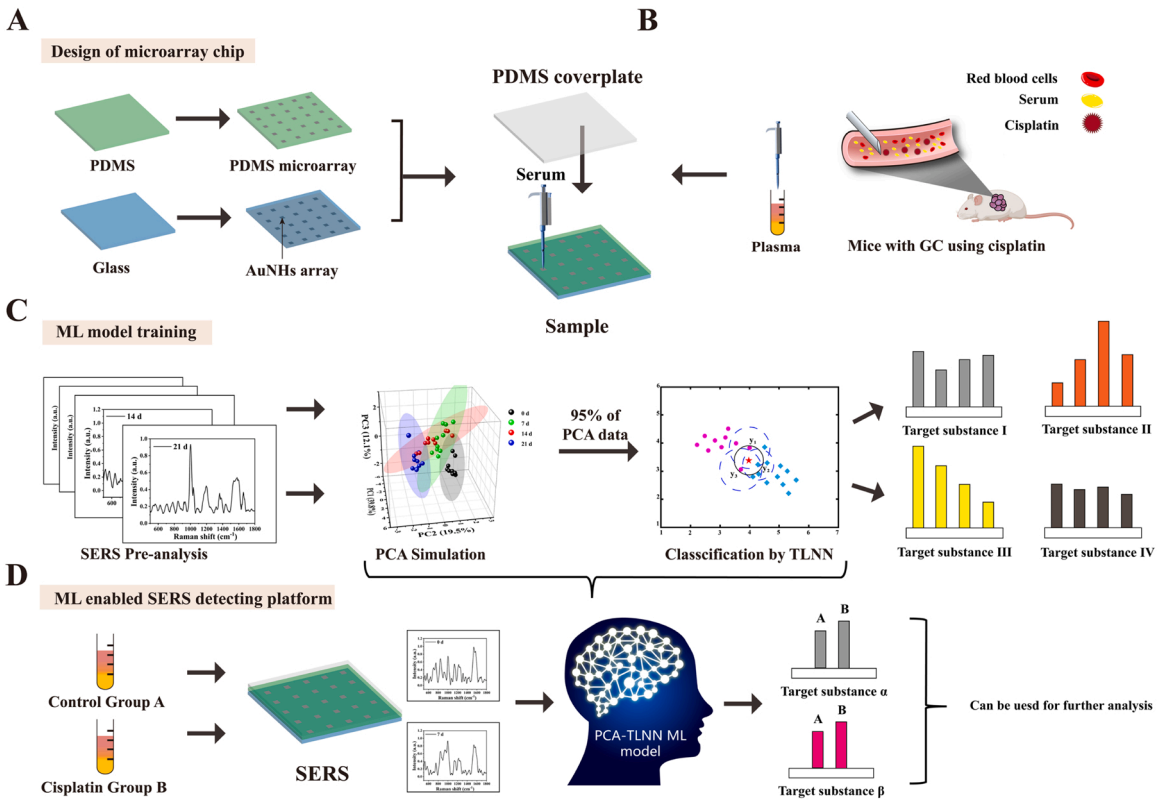

Scheme 1. Schematic illustration of the SERS analysis platform for label-free detection and identification of cisplatin-treated GC with the aid of PCA-TLNN modelling. (A) Design of the microarray chip and (B) detection of SERS spectra of serum from GC mice at different treatment stages. (C) PCA-TLNN model training and (D) analysis of SERS spectra of serum by PCA-TLNN model.

conventional Raman scattering, with an enhancement factor (EF) of up to 108 [16–20]. SERS also has a strong resistance to external interference, indicating that it is suitable for detecting biological samples containing water. The electromagnetic mechanism (EM) model, which generally states that the SERS effect originates from an enhancement caused by the optical excitation of localised surface plasmon resonance (LSPR), has been widely accepted as the main mechanism [21–23]. Because the interactions of light and biomolecules with metal substrates directly impact the increased Raman signal, SERS-active substrates are crucial. Numerous efforts have been made to fabricate new SERS substrates with long-term stability and high enhancement capability. Au nano-hexagon (AuNH) arrays, self-assembled at the liquid-air interface or liquid-liquid interface, are cost-effective and versatile plasmonic nanostructures that have been applied to improve SERS sensitivity [24, 25]. The sharp edges and tips of the hexagons can generate an electric field enhancement, and a highly enhanced electric field can be obtained in the spaces between adjacent AuNHs, thereby achieving good SERS performance.

Serum samples are unique in nature and are easily affected by other factors in the exposed environment, thus leading to changes in peak positions and intensities of SERS spectra. To overcome the above problems in serum SERS testing and avoid contamination of serum by the external environment, combining SERS with a microfluidic chip may provide a new idea. Moreover, the interpretation of similar spectra is another challenge. Multivariate statistical analysis methods, such as principal component analysis (PCA), partial least squares (PLS), and PCA-k-nearest neighbours (KNN), are methods that can unlock the value of data, and are often used to handle large volumes of data. PCA is a statistical analysis method used to compress data and obtain key feature information. After obtaining the SERS spectra of the various groups, PCA generates score and loading plots that maximise the covariance of the spectral data to visualise the dataset and identify features [26,27]. Specifically, PCA is applied to compress the original SERS spectral data and project them onto a lower dimension generated by the principal components (PCs). The PCA score plots representations of the first few PCs, demonstrating the clustering patterns of various groups. Simultaneously, the PCA loading plots from a series of principal components (PCs) can capture valuable information to be considered during the differentiation of SERS spectra. Although the characteristics of the extracted spectra are more abundant than those of a single Raman peak analysis, the recognition ability of PCA is still insufficient for distinguishing the SERS spectra of different groups. Recently, K-Nearest Neighbor (KNN) combined with Principal Component Analysis (PCA) have frequently been used together with spectroscopy in disease diagnostics [28]. The basic idea of the traditional PCA-KNN model is to determine the class label of a test sample based on the nearest neighbour (NN) rule. However, the neighbourhood structure and the similarity metric of the test sample in the NN rule are too unitary, which affects the accurate classification of spectral data [29,30]. The accuracy, sensitivity, and specificity of these traditional models for identifying similar SERS spectra remain insufficient. Therefore, it is necessary to adopt a model with better classification performance.

Herein, we report a label-free SERS analysis platform to assess the efficacy of cisplatin in GC, using a PCA-two-layer nearest neighbour (TLNN) method to guide spectral processing. First, cleaned AuNH substrates were fabricated into chip form to prepare a microarray chip, giving the analysis platform high throughput and portability. A polydimethylsiloxane (PDMS) cover was prepared to provide an enclosed reaction space for isolation from the outside environment (Scheme 1A). Then, a GC subcutaneously xenografted growing human tumour model in mice treated with cisplatin was established, and SERS spectra of serum were obtained at different time points after treatment (Scheme 1 B). After background removal, smoothing, baseline correction, and normalisation of the spectral data, PCA was applied to visualise the

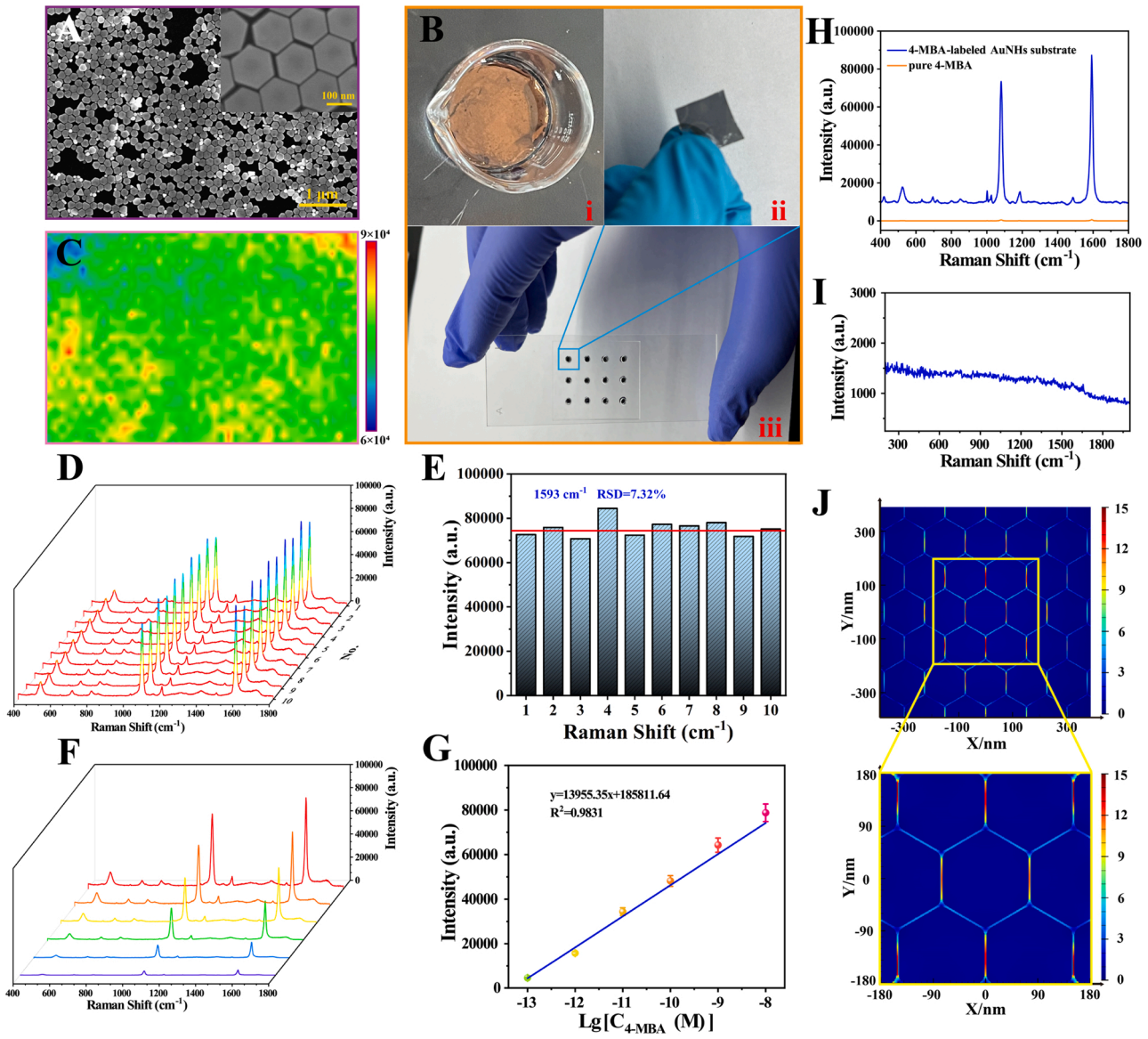

Fig. 1. (A) SEM image of the prepared AuNHs array. Inset: high magnification view. (B) Actual image of (i) Au film, (ii) AuNHs array on glass and (iii) prepared microarray-structural chip. (C) SERS mapping of 4-MBA signal on the prepared AuNHs array and the colour scheme of the signal intensity at 1593 cm^{-1} ranging from blue (lowest intensity) to red (highest intensity) was applied. (D) SERS spectra of 10 different spots selected randomly on the AuNHs array and the (E) corresponding histogram of the peak intensity at 1593 cm^{-1}. (F) SERS spectra of 4-MBA with different concentrations (10^{-8} M, 10^{-9} M, 10^{-10} M, 10^{-11} M, 10^{-12} M and 10^{-13} M) using the prepared AuNHs substrate. (G) Corresponding calibration curves for 4-MBA. (H) SERS spectra of 4-MBA (10^{-8} M) on the AuNHs substrate (blue curve) and 4-MBA (10^{-2} M) on the glass (yellow curve). (I) SERS spectra of AuNHs substrate treated with 0.1 M KI. (J) FDTD simulation of the AuNHs substrate.

dataset and extract features (Scheme 1C). Finally, using the PCA-TLNN algorithm, a SERS spectral identification model for different treatment stages was constructed, followed by a comparison with traditional PCA-KNN (Scheme 1D). The PCA-TLNN model may be considered a good substitute for traditional PCA-KNN and can be used in spectral classification for prognosis. To the best of our knowledge, this is the first report on label-free detection and identification of disease treatment and prognosis using SERS assisted by PCA-TLNN modelling.

2. Results and discussion

2.1. Characterization of microarray chip

AuNHs were synthesised by reducing $AuCl^{4-}$ to Au^{0} using ascorbic acid (AA). Fig. S1 demonstrates that the prepared AuNHs had a uniform size of 87 nm and that their SERS enhancement was satisfactory. The AuNH substrate was synthesised via the self-assembly of AuNHs at a liquid–liquid interface (Fig. 1A). After the addition of n-hexane, a dense metallic lustre nanofilm is observed (Fig. 1B(i)). A glass substrate hydrophilised by piranha solution was used to transform the nanofilm (Fig. 1B(ii)). Thereafter, the AuNH substrate was embedded into a glass slide by laser etching, and a microarray chip was prepared (Fig. 1B(iii)) according to Scheme 1 and Fig. S3. After preparation of the microarray chip, SERS mapping measurements were performed on the AuNH substrate to demonstrate the homogeneity of the SERS signal. The results indicate that most of the area is green (mid-scale), despite some red (high intensity) and blue (low intensity) regions, indicating outstanding signal uniformity across a large area of the AuNH array. The ten SERS spectra recorded via spot-to-spot scanning shown in Fig. 1D are highly similar, and the relative standard deviation (RSD) of the peak intensity at 1593 cm^{-1} is 7.32% (Fig. 1E), further demonstrating outstanding uniformity. Sensitivity was also assessed as another critical feature, and

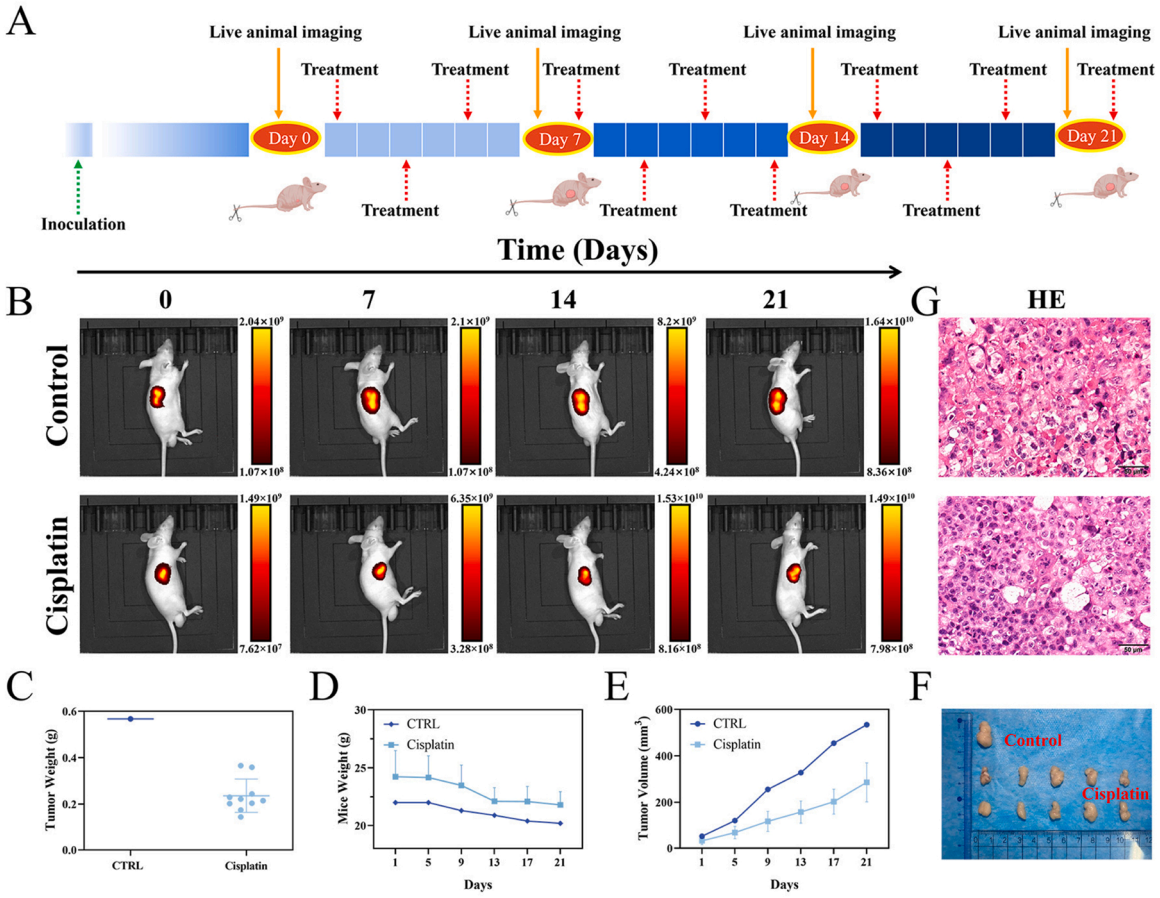

Fig. 2. (A) Schematic illustration of cisplatin-treated GC mice model establishment. (B) Growth of cisplatin group recorded on 0, 7, 14, and 21 days after cisplatin treatment and the growth of control group. (C) Xenograft tumor weight. (D) Body weights of nude mice bearing BGC-823 cells. (E) Volume of the xenograft tumours. (F) Appearance of the xenograft tumours. (G) Hematoxylin and eosin (H&E) staining.

the SERS spectra of 4-mercaptobenzoic acid (4-MBA) at different concentrations were measured (Fig. 1F). The peak intensity at 1593 cm^{-1} (y) versus the logarithm of the 4-MBA concentration (x) was fitted as $y = 13955.35x + 185811.64$, with a correlation coefficient (R^2) of 0.9831 (Fig. 1G), showing a shallow limited detection of 42.1 fM. Thus, the proposed AuNH array presents satisfactory sensitivity, and the enhancement factor (EF) was calculated to be 2.3×10^8 (Fig. 1H). Because of surfactants and reductants remaining on the surface after synthesising the AuNH array, which may interfere with the SERS test results, cleaning with 0.1 M KI was performed [31]. As shown in Fig. 1I, a clean substrate was obtained with no apparent background resulting from iodide adsorbed on the AuNH surface via Au-I bonds and replacing existing impurities. Fig. 1J shows the finite-difference time-domain (FDTD) simulated EM field distribution of the AuNH array, indicating that "hot spots" are primarily distributed around the sharp edges and tips. More importantly, the amplified EM field extends into the junction between adjacent AuNHs, indicating that the preparation of AuNH substrates via self-assembly could offer more significant SERS enhancement. Fig. S4 indicates that PDMS coverage has no obvious influence on the sample signal. Thus, a microarray chip was prepared with excellent uniformity, sensitivity, and cleanliness.

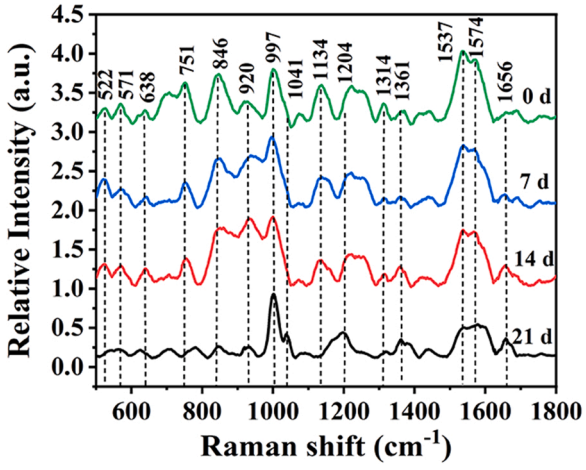

Fig. 3. Mean normalised spectra of serum from GC mice treated with cisplatin for 0, 7, 14, and 21 d.

2.2. *In vivo tumour therapy*

Human gastric cancer BGC-823 cells were injected subcutaneously into BALB/c nude mice, and tumours were visible at the injection point approximately one week later. This time was set as day 0. The treatment group was treated with cisplatin, and a schematic illustration is shown in Fig. 2A. Throughout the experiment, the growth of mice and tumours were monitored using a small animal live imaging instrument throughout the experiment (Fig. S2, Supporting Information) and typical images at four time points are shown in Fig. 2B. The body weights of the mice were recorded (Fig. 2D), and the volume of the subcutaneous tumours was measured and calculated (Fig. 2E). On day 21, the mice from each group were sacrificed. Tumours were harvested (Fig. 2F) and weighed (Fig. 2C). Transplantation tumours were

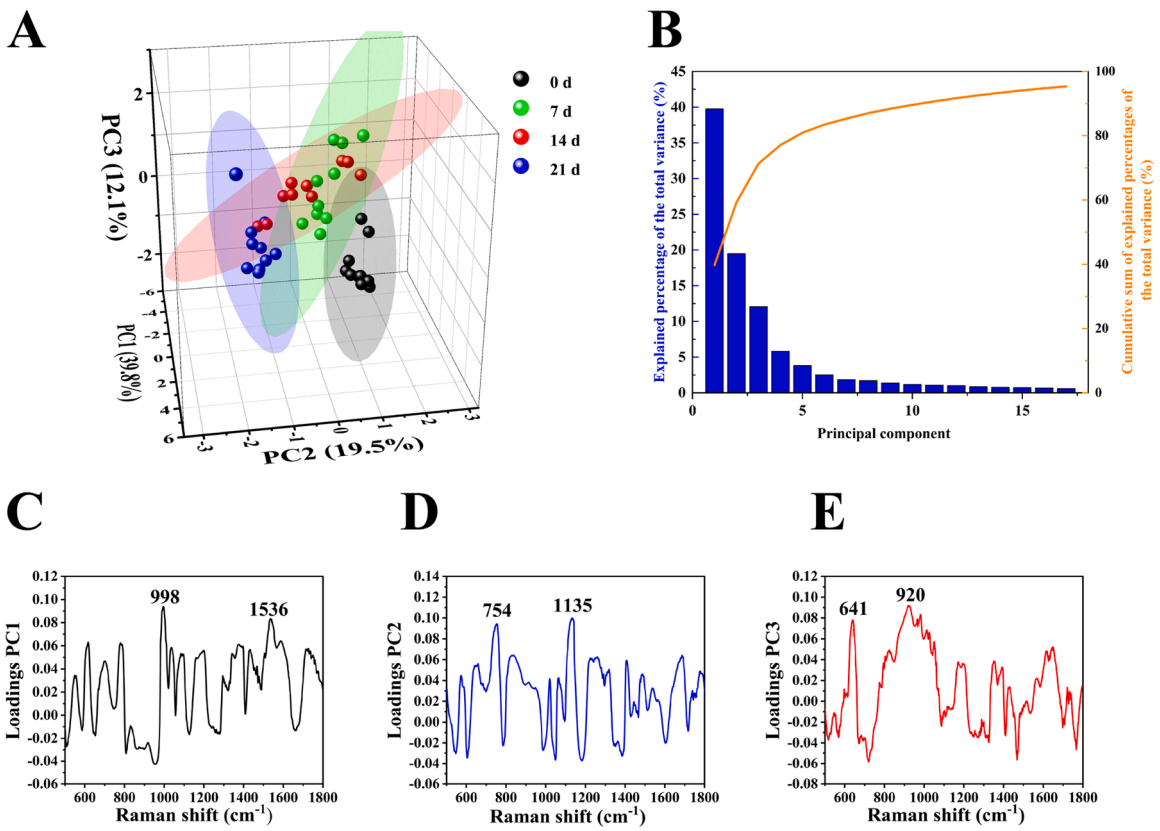

Fig. 4. (A) The PCA score plot for the SERS spectra of the serum from GC mice at different treatment stages. (B) Scree plot of the variation of component number with the calculated eigenvalues for SERS spectra of the serum. (C) Loadings plot of PC1. (D) Loadings plot of PC2. (D) Loadings plot of PC3.

embedded in paraffin and sectioned continuously for hematoxylin and eosin (H&E) staining (Fig. 2G). Under the microscope, the tumour cells were disarranged and disordered, with the nucleus enlarged and deeply stained, matching the characteristics of tumour cells. Compared to the control group, cisplatin treatment significantly inhibited xenograft tumour growth.

2.3. Comparison of SERS spectra of the serum GC mice at different treatment stages

As a direct detection method, serum samples were dropped onto the prepared microarray chip and measured using a confocal Raman spectrometer. The raw SERS spectra were preceded by smoothing and subtracting background normalisation to obtain the spectra of serum from GC mice treated with cisplatin for 0, 7, 14, and 21 d (Fig. S5–S8, Supporting Information). Thereafter, for a direct comparison of the SERS spectra at different treatment stages, the intensity of the serum spectra was normalised to obtain a relative intensity between 0 and 1. Fig. 3 illustrates a stack of the mean normalised spectra of the different treatment stages. These spectra are the average normalised SERS spectra of the mice. The GC mice before treatment clearly show spectral features that are different from those after treatment, whereas the GC mice during cisplatin treatment show similar spectral features. The most outstanding characteristic peaks of the differences are marked in the mean normalised SERS spectra by dotted lines. Detailed assignment of the characteristic peaks is shown in Table S1.

As shown in Fig. 3, the relative intensity of the characteristic peaks at 522 cm^{-1} (S–S disulphide stretching in proteins, phosphatidylserine), 571 cm^{-1} (tryptophan/cytosine), 638 cm^{-1} ((C–S) gauche (amino acid methionine)), 751 cm^{-1} (symmetric breathing of tryptophan (protein assignment)), 846 cm^{-1} (monosaccharides (α-glucose), (C–O–C) skeletal mode, disaccharide (maltose), (C–O–C) skeletal mode), 920 cm^{-1} (C–C stretch of proline ring/glucose/lactic acid, C–C, praline ring (collagen assignment)), 1134 cm^{-1} (fatty acid, (C–C) skeletal of acyl backbone in lipid), 1537 cm^{-1} (amide carbonyl group vibrations and aromatic hydrogens), and 1574 cm^{-1} (ring breathing modes in the DNA bases G and A) show a reverse decreasing trend during cisplatin treatment. However, the peaks at 997 cm^{-1} ((CH deformation) carbohydrates), 1361 cm^{-1} (guanine (N7, B, Z-marker), 1656 cm^{-1} ((C═C)cis (phospholipids), and Amide I (collagen assignment)), found to initially decrease in relative intensity, gradually increased with extension of the treatment time. Furthermore, new characteristic peaks at 1042 cm^{-1} (proline (collagen assignment)) and 1204 cm^{-1} (amide III and CH_2 wagging vibrations from glycine backbone and proline side chain collagen) were SERS spectral features that were found in the mean normalised spectrum after 21 days of treatment with cisplatin samples, but not at the other treatment stages. The increase or decrease in the intensity of these characteristic peaks reflects the variation in relative concentration of biochemical components in the serum, and are closely related to the treatment stage of gastric cancer. The fingerprint characteristics of SERS spectra have important clinical significance in the treatment and prognosis of gastric cancer. This summarises our preliminarily exploration of the differences in the spectra of serum from GC mice before and after treatment.

2.4. Multivariate analysis

The SERS spectra of serum contain multi-dimensional data with rich information, and many irrelevant characteristic peaks could affect discrimination. To further distinguish the SERS spectra of the different treatment stages, this study used the multivariate analysis method PCA-TLNN. PCA is a statistical method that was used to capture key features from SERS spectra. Key eigenvectors of the SERS spectra were selected after dimension reduction. PC1 is the largest eigenvector and shows the

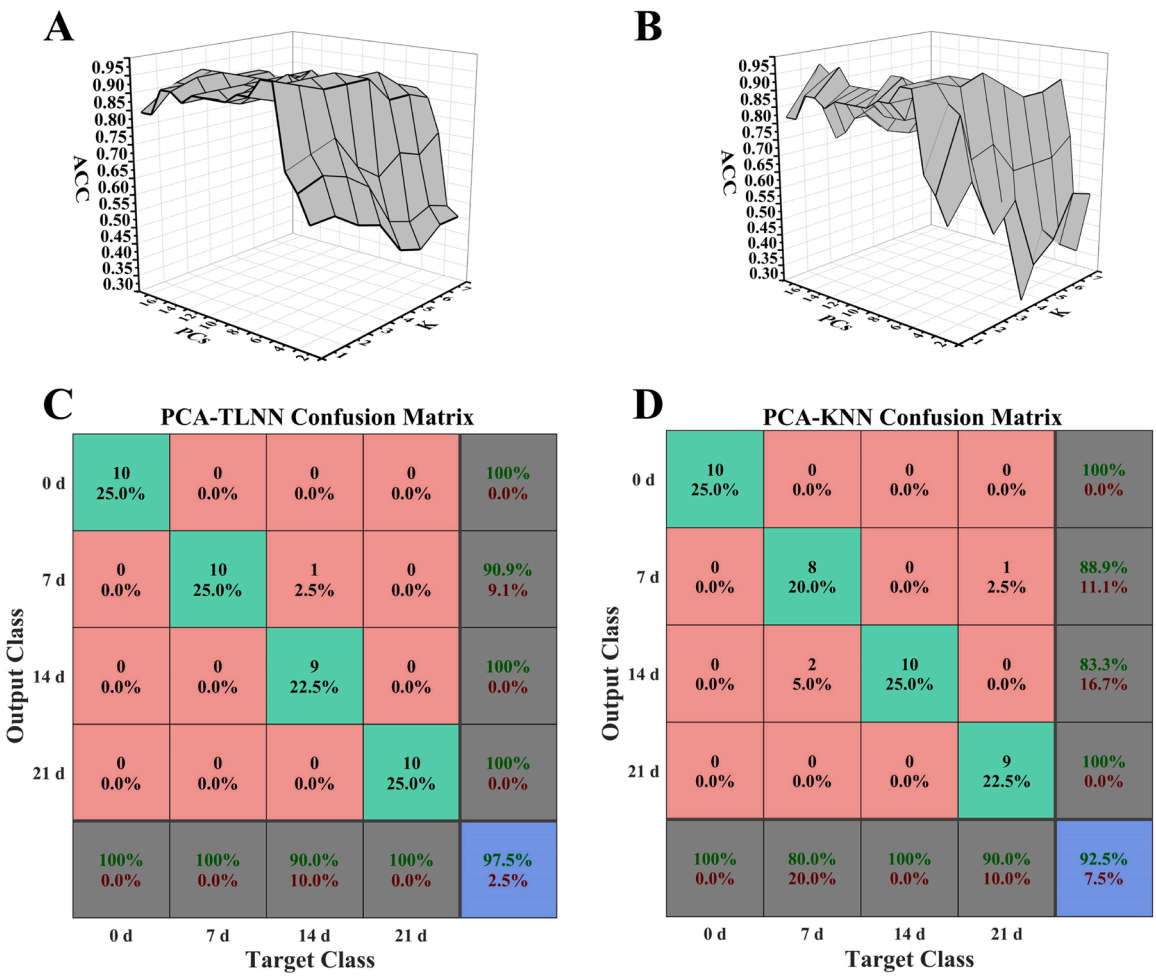

Fig. 5. (A) Accuracy of PCA-TLNN using different PCs and different K values. (B) Accuracy of PCA-KNN using different PCs and different K values. (C) PCA-TLNN confusion matrix. (D) PCA-KNN confusion matrix.

direction of the largest differences between the SERS spectra. PC2 is the second-largest eigenvector, which is orthogonal to PC1 [32,33]. The PCA score plot, composed of two or three PCs, can easily identify key changes in the SERS spectra. As shown in Fig. 4A, the SERS spectral data of the serum from GC mice at different treatment stages were used to create a score plot of the first three PCs. It can be seen that most of the presented variance is accounted for by PC1, PC2 and PC3 (39.8%, 19.5% and 12.1%, respectively), accounting for a total of 71.4% of the total variance [34]. Most of the projection points in each stage can be surrounded by an obvious 95%-confidence ellipsoid. In the PCA score plot, each point represents a mouse at each stage. The SERS spectra at 0 and 21 d are distinguishable, and they are well divided into two distinct groups. This is primarily attributed to differences in the biochemical composition of the serum. After 7 d of cisplatin treatment, the 7-d group is closer to the 0-d group. When the GC mice were treated for 14 d, their group is far from the 0-d group and partially overlaps the 7-d and 21-d groups. These results are consistent with the spectral analysis of the four treatment stages. The scree plot in Fig. 4B shows the variation of the component number with the calculated eigenvalues for the SERS spectra of the serum. This clearly shows the proportion of the total variance accounted for by each principal component, with PC1 accounting for the highest proportion. The first 15 principal components accounting for 95% of the variance were selected to replace the original characteristic spectrum to reduce the number of variables input into the TLNN.

The key spectral features for distinguishing GC mice at different treatment stages were captured by evaluating PC1, PC2, and PC3 loading plots. The high and low load values corresponded to each Raman shift in PC loading, which was the key to determining the direction of maximum variance among the SERS spectra of different treatment stages. The corresponding PC1 scores mainly originated from the positive peaks at approximately 998 cm^{-1} and 1536 cm^{-1} (Fig. 4C). Other prominent spectroscopic features were located at 754, 1135, 641, and 920 cm^{-1}, which can be observed in PC2 loading (Fig. 4D) and PC3 loading (Fig. 4E). The characteristic peak at 998 cm^{-1} is assigned to (CH deformation) carbohydrates. The characteristic peaks at 641, 754, 920, 1135, and 1536 cm^{-1} are related to vibrations in nucleic acids, proteins, and lipids. The vibration peaks of these substances decreased after cisplatin treatment, indicating a decrease in their concentration in the serum. We speculate that this is due to apoptosis or necrosis of a large number of cells during the treatment, resulting in nucleoplasm condensation, chromatin degradation, and proteolytic enzyme activation. These results indicate that PCA-assisted SERS can effectively identify and distinguish between GC mice before and after treatment.

After PCA processing, we selected the first 15 PCs which accounted for 95% of the total variance, and used them as features for the PCA-TLNN. The TLNN is a neighbourhood selection method based on two-level neighbourhood information [35]. The classification principle of TLNN is illustrated in Fig. S9. To analyse the performance of the PCA-TLNN model, it was compared with traditional PCA-KNN modelling. Using LOOCV (leave one out cross-validation), the accuracy of PCA-TLNN and PCA-KNN based on different PCs and K values was determined, as shown in Fig. 5A and Fig. 5B. It is clear that the overall accuracy of PCA-TLNN is higher than that of PCA-KNN and is not sensitive to the selection of the K value [36,37]. The discrimination

accuracy was the highest when the K and PC values were 3 and 7, respectively. These two values were input into PCA-TLNN and PCA-KNN to calculate the confusion matrix. An accuracy of 97.5% (39/40) was achieved in the PCA-TLNN confusion matrix (Fig. 5C), and an accuracy of 92.5% (37/40) was achieved in the PCA-KNN confusion matrix (Fig. 5D). Here, only one SERS spectrum (from the 14-d group) was incorrectly classified as a 7-d group in the PCA-TLNN. The SERS spectra of one 21-d group and two 14-d groups were incorrectly classified as 7-d and 14-d groups in the PCA-KNN, respectively. This result demonstrates the good recognition ability of the TLNN method for the SERS spectra at 0, 7, 14, and 21 d. We also analysed the accuracy, sensitivity, and specificity of PCA-TLNN and PCA-KNN at 0 d and other groups, 7 d and other groups, 14 d and other groups, and 21 d and other groups (Table S2, Supporting Information). Compared with PCA-KNN, PCA-TLNN has significant advantages in the analysis of SERS spectral data. It is concluded that PCA-TLNN can help reveal important spectral information and assist in the staging of GC treatment.

3. Conclusions

In conclusion, we developed a novel strategy combining SERS technology and PCA-TLNN to rapidly detect cisplatin-treated GC mice without labelling. This approach relied on a microarray chip fabricated from AuNH substrates, which exhibited superior portability and SERS activity, stability, and uniformity. Using a microarray chip as the sensing platform, high-quality SERS signals of the serum of GC mice at different treatment stages were acquired, and a series of characteristic peaks representative of various biomolecules were detected. The PCA-TLNN SERS spectra successfully differentiated GC mice at different treatment stages. The most prominent spectral features for distinguishing different treatment stages were observed for PC loading, including those at 641, 754, 998, 920, 1135, and 1536 cm-1. Compared with traditional PCA-KNN, the PCA-TLNN model based on principal component variables had better accuracy, sensitivity, and specificity for spectral classification. The PCA-TLNN can be considered a good alternative to the well-established discriminant model. The proposed method combining SERS with PCA-TLNN is a powerful and promising tool for label-free serum detection in a liquid environment and indicates promising potential for application in cancer treatment, specific disease diagnosis, and the development of individual therapeutic strategies.

CRediT authorship contribution statement

Dawei Cao: Methodology, Validation, Formal analysis, Investigation, Data curation, and Writing of original draft. **Hechuan Lin:** Investigation, Resources, and Data curation. **Ziyang Liu:** Methodology, Software, and Validation. **Jiaji Qiu:** Formal analysis. **Shengjie Ge:** Formal analysis, Investigation, and Data curation. **Weiwei Hua:** Methodology, Resources, and Validation. **Xiaowei Cao:** Writing – review and editing, Project administration, and Funding acquisition. **Yayun Qian:** Writing – review and editing, Supervision, and Project administration. **Huiying Xu:** Review and editing, Visualisation, Supervision, Project administration, and Funding acquisition. **Xinzhong Zhu:** Review and editing, Visualisation, Supervision, Project administration, and Funding acquisition.

Declaration of Competing Interest

The authors declare that they have no known competing financial interests or personal relationships that could have appeared to influence the work reported in this paper.

Data availability

Data will be made available on request.

Acknowledgment

This work was supported by the Natural Science Foundation of China (project no. 61976196), Outstanding Talents of “Ten Thousand Talents Plan” in Zhejiang Province (project no. 2018R51001), the Zhejiang Provincial Natural Science Foundation of China (project no. LZ22F030003), the Social Development Foundation of Jiangsu (No. BE2018684), the Major Programs of Natural Science Foundation of Higher Education in Jiangsu Province (19KJA480003) and the Administration of Traditional Chinese Medicine Project of Jiangsu Province (MS2021081), the High-end Talent Support Program of Yangzhou University, the QingLan Project of Yangzhou University.

Appendix A. Supporting information

Supplementary data associated with this article can be found in the online version at doi:10.1016/j.snb.2022.132903.

References

[1] H. Zhang, R. Li, Y. Cao, Y. Gu, C. Lin, X. Liu, K. Lv, X. He, H. Fang, K. Jin, Y. Fei, Y. Chen, J. Wang, H. Liu, H. Li, H. Zhang, H. He, W. Zhang, Ann. Surg. 275 (2022) E626–E635.
[2] D. Chen, Z. Liu, W. Liu, M. Fu, W. Jiang, S. Xu, G. Wang, F. Chen, J. Lu, H. Chen, X. Dong, G. Li, G. Chen, S. Zhuo, J. Yan, Nat. Commun. 12 (2021).
[3] Y. Kang, L. Chen, M. Ryu, D. Oh, S. Oh, H. Chung, K. Lee, T. Omori, K. Shitara, S. Sakuramoto, I. Chung, K. Yamaguchi, K. Kato, S. Sym, S. Kadowaki, K. Tsuji, J. Chen, L. Bai, S. Oh, Y. Choda, H. Yasui, K. Takeuchi, Y. Hirashima, S. Hagihara, N. Boku, Lancet Oncol. 23 (2022) 234–247.
[4] F. Huang, S. Yu, Asian J. Surg. 41 (2018) 210–215.
[5] Z. Tan, Med. Sci. Monit. 25 (2019) 3537–3541.
[6] L. Shen, Y. Shan, H. Hu, T. Price, B. Sirohi, K. Yeh, Y. Yang, T. Sano, H. Yang, X. Zhang, S. Park, M. Fujii, Y. Kang, L. Chen, Lancet Oncol. 14 (2013) E535–E547.
[7] P. Zheng, L. Chen, X. Yuan, Q. Luo, Y. Liu, G. Xie, Y. Ma, L. Shen, J. Exp. Clin. Canc. Res. 36 (2017).
[8] M. Orditura, G. Galizia, V. Sforza, V. Gambardella, A. Fabozzi, M. Laterza, F. Andreozzi, J. Ventriglia, B. Savastano, A. Mabilia, E. Lieto, F. Ciardiello, F. De Vita, World J. Gastroenterol. 20 (2014) 1635–1649.
[9] L. Necula, L. Matei, D. Dragu, A. Neagu, C. Mambet, S. Nedeianu, C. Bleotu, C. Diaconu, M. Chivu-Economescu, World J. Gastroenterol. 25 (2019) 2029–2044.
[10] J. Lin, R. Chen, S. Feng, J. Pan, Y. Li, G. Chen, M. Cheng, Z. Huang, Y. Yu, H. Zeng, Nanomed. -Nanotechnol. 7 (2011) 655–663.
[11] C. Camp, Y. Lee, J. Heddleston, C. Hartshorn, A. Walker, J. Rich, J. Lathia, M. Cicerone, Nat. Photonics 8 (2014) 627–634.
[12] X. Wang, S. Huang, S. Hu, S. Yan, B. Ren, Nat. Rev. Phys. 2 (2020) 253–271.
[13] K. Xu, R. Zhou, K. Takei, M. Hong, Adv. Sci. 6 (2019).
[14] R. Zhang, Y. Zhang, Z. Dong, S. Jiang, C. Zhang, L. Chen, L. Zhang, Y. Liao, J. Aizpurua, Y. Luo, J. Yang, J. Hou, NATURE 498 (2013) 82–86.
[15] D. Zhang, H. Pu, L. Huang, D. Sun, Trends Food Sci. Technol. 109 (2021) 690–701.
[16] D. Cialla, A. Marz, R. Bohme, F. Theil, K. Weber, M. Schmitt, J. Popp, Anal. Bioanal. Chem. 403 (2012) 27–54.
[17] B. Sharma, R. Frontiera, A. Henry, E. Ringe, R. Van Duyne, Mater. Today 15 (2012) 16–25.
[18] C. Zong, M. Xu, L. Xu, T. Wei, X. Ma, X. Zheng, R. Hu, B. Ren, Chem. Rev. 118 (2018) 4946–4980.
[19] M. Cardinal, E. Ende, R. Hackler, M. McAnally, P. Stair, G. Schatz, R. Van Duyne, Chem. Soc. Rev. 46 (2017) 3886–3903.
[20] V. Moisoiu, S.D. Iancu, A. Stefancu, T. Moisoiu, B. Pardini, M.P. Dragomir, N. Crisan, L. Avram, D. Crisan, I. Andras, D. Fodor, L.F. Leopold, C. Socaciu, Z. Bálint, C. Tomuleasa, F. Elec, N. Leopold, Colloids Surf. B 208 (2021), 112064.
[21] C. Zhang, C. Lia, J. Yu, S. Jiang, S. Xu, C. Yang, Y. Liu, X. Gao, A. Liu, B. Man, Sens. Actuators B Chem. 258 (2018) 163–171.
[22] S. Yang, J. Yao, Y. Quan, M. Hu, R. Su, M. Gao, D. Han, J. Yang, Light Sci. Appl. 9 (2020).
[23] D. Wu, J. Li, B. Ren, Z. Tian, Chem. Soc. Rev. 37 (2008) 1025–1041.
[24] H. Tajarenejad, M. Ansari, S. Akbari, H. Yazdanfar, S. Hamidi, Biomed. Opt. Express 12 (2021) 6013–6023.
[25] S. D'Souza, R. Ogbodu, T. Nyokong, J. Mol. Struct. 1099 (2015) 551–559.
[26] J. Park, M. Hwang, B.H. Choi, H. Jeong, J. Jung, H.K. Kim, S. Hong, J. Park, Y. Choi, Anal. Chem. 89 (2017) 6695–6701.
[27] H. Shin, H. Jeong, J. Park, S. Hong, Y. Choi, ACS Sens. 3 (2018) 2637–2643.
[28] U. Parlatan, M.T. Inanc, B.Y. Ozgor, E. Oral, E. Bastu, M.B. Unlu, G. Basar, Sci. Rep. 9 (2019) 19795.
[29] Q.B. Li, W.J. Li, J.L. Zhang, Z. Xu, Analyst 143 (2018) 2807–2811.
[30] J. Chauvin, R. Duran, K. Tavakolian, A. Akhbardeh, N. MacKinnon, J.W. Qin, D. E. Chan, C.S. Hwang, I. Baek, M.S. Kim, R.B. Isaacs, A.G. Yilmaz, J. Roungchun, R. S. Hellberg, F. Vasefi, Appl. Sci. 11 (2021) 10628.
[31] J.Y. Huang, C. Zong, L.J. Xu, Y. Cui, B. Ren, Chem. Commun. 47 (2011) 5738–5740.

[32] S.K. Gahlaut, D. Savargaonkar, C. Sharan, Sarjana Yadav, P. Mishra, J.P. Singh, Anal. Chem. 92 (2020) 2527–2534.
[33] S.S. Du, M.K. Su, Y.F. Jiang, F.F. Yu, Y. Xu, X.F. Lou, T. Yu, H.L. Liu, ACS Sens. 4 (2019) 1798–1805.
[34] E. Witkowska, A.M. Łasica, K. Nicinski, J. Potempa, A. Kaminska, ACS Sens. 6 (2021) 1621–1635.
[35] Y.K. Wang, Z.B. Pan, J. Dong. Knowl. -Based Syst. 235 (2022), 107604.
[36] V.E. Almeida, D.D. Fernandes, P.H.G.D. Diniz, A.A. Gomes, G. Veras, R.K. H. Galvao, M.C.U. Araujo, Food Chem. 363 (2021), 130296.
[37] S.Y.S. Adade, H. Lin, H. Jiang, S.A. Haruna, A.O. Barimah, M. Zareef, A. A. Agyekum, N.A.N. Johnson, M.M. Hassan, H.H. Li, Q.S. Chen, Food Chem. 388 (2022), 132973.

Dawei Cao is currently a graduate student at College of Mathematics and Computer Science, Zhejiang Normal University.

Hechuan Lin is currently a graduate student at College of Mathematics and Computer Science, Zhejiang Normal University.

Ziyang Liu is currently a graduate student at College of Mathematics and Computer Science, Zhejiang Normal University.

Jiaji Qiu is currently a graduate student at College of Mathematics and Computer Science, Zhejiang Normal University.

Shengjie Ge is currently a graduate student at the Medical School of Yangzhou University.

Weiwei Hua is currently a graduate student at the Medical School of Yangzhou University.

Xiaowei Cao is a Professor in Institute of Translational Medicine, Medical College, Yangzhou University, Yangzhou.

Yayun Qian is a Professor in Institute of Translational Medicine, Medical College, Yangzhou University, Yangzhou.

Huiying Xu is a Professor at College of Mathematics and Computer Science, Zhejiang Normal University. Currently.

Xinzhong Zhu is a Professor at College of Mathematics and Computer Science, Zhejiang Normal University. Currently.